

1 **MitoChime: A Machine Learning Pipeline for**
2 **Detecting PCR-Induced Chimeras in**
3 **Mitochondrial Illumina Reads**

4 A Special Project Proposal
5 Presented to
6 the Faculty of the Division of Physical Sciences and Mathematics
7 College of Arts and Sciences
8 University of the Philippines Visayas
9 Miagao, Iloilo

10 In Partial Fulfillment
11 of the Requirements for the Degree of
12 Bachelor of Science in Computer Science

13 by

14 Duranne Duran
15 Yvonne Lin
16 Daniella Pailden

17 Adviser
18 Francis D. Dimzon, Ph.D.

19 December 5, 2025

Abstract

21 Next-generation sequencing (NGS) platforms have advanced research but re-
22 main susceptible to artifacts such as PCR-induced chimeras that compromise
23 mitochondrial genome assembly. These artificial hybrid sequences are prob-
24 lematic for small, circular, and repetitive mitochondrial genomes, where they
25 can generate fragmented contigs and false junctions. Existing detection tools,
26 such as UCHIME, are optimized for amplicon-based microbial community ana-
27 lysis and depend on reference databases or abundance assumptions unsuitable
28 for organellar assembly. To address this gap, this study presents MitoChime,
29 a machine learning pipeline for detecting PCR-induced chimeric reads in *Sar-*
30 *dinella lemuru* Illumina paired-end data without relying on external reference
31 databases.

32 Using simulated datasets containing clean and chimeric reads, we extracted
33 a feature set combining alignment-based metrics (e.g., supplementary align-
34 ments, soft-clipping) with sequence-derived statistics (e.g., k-mer composition,
35 microhomology). A comparative evaluation of supervised learning models
36 identified tree-based ensembles CatBoost and Gradient Boosting as top per-
37 formers, achieving an F1-score of 0.77 and an ROC-AUC of 0.84 on held-out
38 test data. Feature importance analysis highlighted soft-clipping and k-mer
39 compositional shifts as the strongest predictors of chimerism, whereas micro-
40 homology contributed minimally. Integrating MitoChime as a pre-assembly
41 step can aid in streamlining mitochondrial reconstruction pipelines.

42 **Keywords:** Chimera detection, Mitochondrial genome,
Assembly, Machine learning

⁴³ **Contents**

⁴⁴	1 Introduction	1
⁴⁵	1.1 Overview	1
⁴⁶	1.2 Problem Statement	3
⁴⁷	1.3 Research Objectives	4
⁴⁸	1.3.1 General Objective	4
⁴⁹	1.3.2 Specific Objectives	4
⁵⁰	1.4 Scope and Limitations of the Research	5
⁵¹	1.5 Significance of the Research	6
⁵²	2 Review of Related Literature	7
⁵³	2.1 The Mitochondrial Genome	7
⁵⁴	2.1.1 Mitochondrial Genome Assembly	8

55	2.2 PCR Amplification and Chimera Formation	9
56	2.3 Existing Traditional Approaches for Chimera Detection	10
57	2.3.1 UCHIME	11
58	2.3.2 UCHIME2	12
59	2.3.3 CATch	13
60	2.3.4 ChimPipe	14
61	2.4 Machine Learning Approaches for Chimera and Sequence Quality	
62	Detection	15
63	2.4.1 Feature-Based Representations of Genomic Sequences . . .	15
64	2.5 Synthesis of Chimera Detection Approaches	16
65	3 Research Methodology	19
66	3.1 Research Activities	19
67	3.1.1 Data Collection	20
68	3.1.2 Feature Extraction Pipeline	24
69	3.1.3 Machine Learning Model Development	26
70	3.1.4 Model Benchmarking, Hyperparameter Optimization, and	
71	Evaluation	28
72	3.1.5 Feature Importance and Interpretation	29

73	3.1.6 Validation and Testing	30
74	3.1.7 Documentation	31
75	3.2 Calendar of Activities	32
76	4 Results and Discussion	33
77	4.1 Descriptive Analysis of Features	33
78	4.1.1 Exploratory Data Analysis	34
79	4.2 Baseline Classification Performance	35
80	4.3 Effect of Hyperparameter Tuning	37
81	4.4 Detailed Evaluation of Representative Models	38
82	4.4.1 Confusion Matrices and Error Patterns	39
83	4.4.2 ROC and Precision–Recall Curves	40
84	4.5 Feature Importance and Biological Interpretation	42
85	4.5.1 Permutation Importance of Individual Features	42
86	4.5.2 Feature Family Importance	43
87	4.6 Summary of Findings	45
88	A Exploratory Data Analysis	47
89	A.1 Histograms of Key Features	47

⁹⁰ List of Figures

⁹¹	3.1 Process Diagram of Special Project	20
⁹²	4.1 Feature correlation heatmap showing relationships among alignment-derived and sequence-derived variables.	35
⁹³		
⁹⁴	4.2 Test F1 of all baseline classifiers, showing that no single model clearly dominates and several achieve comparable performance. . .	36
⁹⁵		
⁹⁶	4.3 Comparison of test F1 (left) and ROC–AUC (right) for baseline and tuned models. Hyperparameter tuning yields small but consistent gains, particularly for tree-based ensembles.	38
⁹⁷		
⁹⁸		
⁹⁹	4.4 Confusion matrices for the four representative models on the held-out test set. All models show more false negatives (chimeric reads called clean) than false positives.	40
¹⁰⁰		
¹⁰¹		
¹⁰²	4.5 ROC (left) and precision–recall (right) curves for the four representative models on the held-out test set. Tree-based ensembles cluster closely, with logistic regression performing slightly but consistently worse.	41
¹⁰³		
¹⁰⁴		
¹⁰⁵		

106	4.6 Permutation-based feature importance for four representative clas-	
107	sifiers. Clipping and k-mer composition features are generally the	
108	strongest predictors, whereas microhomology and other alignment	
109	metrics contribute minimally.	43
110	4.7 Aggregated feature family importance across four models. Clipping	
111	and k-mer compositional shifts are consistently the dominant con-	
112	tributors, while SA_structure, Micro_homology, and other features	
113	contribute minimally.	45
114	A.1 Histogram plots of six key features comparing clean and chimeric	
115	reads.	48

116 List of Tables

¹²¹ Chapter 1

¹²² Introduction

¹²³ 1.1 Overview

¹²⁴ The rapid advancement of next-generation sequencing (NGS) technologies has
¹²⁵ transformed genomic research by enabling high-throughput and cost-effective
¹²⁶ DNA analysis (Metzker, 2010). Among current platforms, Illumina sequencing
¹²⁷ remains the most widely adopted, capable of producing millions of short reads
¹²⁸ that can be assembled into reference genomes or analyzed for genetic variation
¹²⁹ (Bentley et al., 2008; Glenn, 2011). Despite its high base-calling accuracy,
¹³⁰ Illumina sequencing is prone to artifacts introduced during library preparation,
¹³¹ particularly polymerase chain reaction (PCR)-induced chimeras, which are ar-
¹³² tificial hybrid sequences that do not exist in the true genome (Judo, Wedel, &
¹³³ Wilson, 1998).

¹³⁴ PCR chimeras form when incomplete extension products from one template

anneal to an unrelated DNA fragment and are extended, creating recombinant reads (Qiu et al., 2001). In mitochondrial genome assembly, such artifacts are especially problematic because the mitochondrial genome is small, circular, and often repetitive (Boore, 1999; Cameron, 2014). Even a small number of chimeric or misjoined reads can reduce assembly contiguity and introduce false junctions during organelle genome reconstruction (Dierckxsens, Mardulyn, & Smits, 2017; Hahn, Bachmann, & Chevreux, 2013; Jin et al., 2020). Existing assembly tools such as GetOrganelle and MITObim assume that input reads are largely free of such artifacts (Hahn et al., 2013; Jin et al., 2020). Consequently, undetected chimeras may produce fragmented assemblies or misidentified organellar boundaries. To ensure accurate reconstruction of mitochondrial genomes, a reliable method for detecting and filtering PCR-induced chimeras before assembly is essential.

This study focuses on mitochondrial sequencing data from the genus *Sardinella*, a group of small pelagic fishes widely distributed in Philippine waters. Among them, *Sardinella lemuru* (Bali sardinella) is one of the country's most abundant and economically important species, providing protein and livelihood to coastal communities (Labrador, Agmata, Palermo, Ravago-Gotanco, & Pante, 2021; Willette, Bognot, Mutia, & Santos, 2011). Accurate mitochondrial assemblies are critical for understanding its population genetics, stock structure, and evolutionary history. However, assembly pipelines often encounter errors or fail to complete due to undetected chimeric reads. To address this gap, this research introduces MitoChime, a machine learning pipeline designed to detect and filter PCR-induced chimeric reads using both alignment-based and sequence-derived statistical features. The tool aims to provide bioinformatics laboratories, partic-

₁₆₀ ularly the Philippine Genome Center Visayas (PGC Visayas), with an efficient
₁₆₁ solution for improving mitochondrial genome reconstruction.

₁₆₂ 1.2 Problem Statement

₁₆₃ While NGS technologies have revolutionized genomic data acquisition, the ac-
₁₆₄ curacy of mitochondrial genome assembly remains limited by artifacts produced
₁₆₅ during PCR amplification. These chimeric reads can distort assembly graphs and
₁₆₆ cause misassemblies, with particularly severe effects in small, circular mitochon-
₁₆₇ drial genomes (Boore, 1999; Cameron, 2014). Existing assembly pipelines such
₁₆₈ as GetOrganelle, MITObim, and NOVOPlasty assume that sequencing reads are
₁₆₉ free of such artifacts (Dierckxsens et al., 2017; Hahn et al., 2013; Jin et al., 2020).
₁₇₀ At PGC Visayas, several mitochondrial assemblies have failed or yielded incom-
₁₇₁ plete contigs despite sufficient coverage, suggesting that undetected chimeric reads
₁₇₂ compromise assembly reliability. Meanwhile, existing chimera detection tools such
₁₇₃ as UCHIME and VSEARCH were developed primarily for amplicon-based com-
₁₇₄ munity analysis and rely heavily on reference or taxonomic comparisons (Edgar,
₁₇₅ Haas, Clemente, Quince, & Knight, 2011; Rognes, Flouri, Nichols, Quince, &
₁₇₆ Mahé, 2016). These approaches are unsuitable for single-species organellar data,
₁₇₇ where complete reference genomes are often unavailable. Therefore, there is a
₁₇₈ pressing need for a reference-independent, data-driven tool capable of detecting
₁₇₉ and filtering PCR-induced chimeras in mitochondrial sequencing datasets.

180 **1.3 Research Objectives**

181 **1.3.1 General Objective**

182 This study aims to develop and evaluate a machine learning-based pipeline (Mi-
183 toChime) that detects PCR-induced chimeric reads in *Sardinella lemuru* mito-
184 chondrial sequencing data in order to improve the quality and reliability of down-
185 stream mitochondrial genome assemblies.

186 **1.3.2 Specific Objectives**

187 Specifically, the study aims to:

- 188 1. construct simulated *Sardinella lemuru* Illumina paired-end datasets contain-
189 ing both clean and PCR-induced chimeric reads,
- 190 2. extract alignment-based and sequence-based features such as k-mer compo-
191 sition, junction complexity, and split-alignment counts from both clean and
192 chimeric reads,
- 193 3. train, validate, and compare supervised machine learning models for classi-
194 fying reads as clean or chimeric,
- 195 4. determine feature importance and identify indicators of PCR-induced
196 chimerism,
- 197 5. integrate the optimized classifier into a modular and interpretable pipeline
198 deployable on standard computing environments at PGC Visayas.

¹⁹⁹ **1.4 Scope and Limitations of the Research**

²⁰⁰ This study focuses on detecting PCR-induced chimeric reads in Illumina paired-
²⁰¹ end mitochondrial sequencing data from *Sardinella lemuru*. The decision to re-
²⁰² strict the taxonomic scope to a single species is based on four considerations: to
²⁰³ limit interspecific variation in mitochondrial genome size, GC content, and repeti-
²⁰⁴ tive regions so that differences in read patterns can be attributed more directly to
²⁰⁵ PCR-induced chimerism; to align the analysis with relevant *S. lemuru* sequencing
²⁰⁶ projects at PGC Visayas; to take advantage of the availability of *S. lemuru* mito-
²⁰⁷ chondrial assemblies and raw datasets in public repositories such as the National
²⁰⁸ Center for Biotechnology Information (NCBI), which facilitates reference selection
²⁰⁹ and benchmarking; and to develop a tool that directly supports local studies on
²¹⁰ *S. lemuru* population structure and fisheries management.

²¹¹ The study emphasizes `wgsim`-based simulations and selected empirical mito-
²¹² chondrial datasets from *S. lemuru*. It excludes naturally occurring chimeras, nu-
²¹³ clear mitochondrial pseudogenes (NUMTs), and large-scale assembly rearrange-
²¹⁴ ments in nuclear genomes. Feature extraction is restricted to low-dimensional
²¹⁵ alignment and sequence statistics, such as k-mer frequency profiles, GC content,
²¹⁶ read length, soft and hard clipping metrics, split-alignment counts, and map-
²¹⁷ ping quality, rather than high-dimensional deep learning embeddings. This de-
²¹⁸ sign keeps model behaviour interpretable and ensures that the pipeline can be
²¹⁹ run on standard workstations at PGC Visayas. Testing on long-read platforms
²²⁰ (e.g., Nanopore, PacBio) and other taxa is outside the scope of this project; the
²²¹ implemented pipeline is evaluated only on short-read *S. lemuru* datasets.

²²² Other limitations in this study include the following: simulations with varying

223 error rates were not performed, so the effect of different sequencing errors on model
224 performance remains unexplored; alternative parameter settings, including k-mer
225 lengths and microhomology window sizes, were not systematically tested, which
226 could affect the sensitivity of both k-mer and microhomology feature detection as
227 well as the identification of chimeric junctions; and the machine learning models
228 rely on supervised training with labeled examples, which may limit their ability
229 to detect novel or unexpected chimeric patterns.

230 1.5 Significance of the Research

231 This research provides both methodological and practical contributions to mito-
232 chondrial genomics and bioinformatics. First, MitoChime detects PCR-induced
233 chimeric reads prior to genome assembly, with the goal of improving the con-
234 tiguity and correctness of *Sardinella lemuru* mitochondrial assemblies. Second,
235 it replaces informal manual curation with a documented workflow, improving au-
236 tomation and reproducibility. Third, the pipeline is designed to run on computing
237 infrastructures commonly available in regional laboratories, enabling routine use
238 at facilities such as PGC Visayas. Finally, more reliable mitochondrial assemblies
239 for *S. lemuru* provide a stronger basis for downstream applications in the field of
240 fisheries and genomics.

²⁴¹ **Chapter 2**

²⁴² **Review of Related Literature**

²⁴³ This chapter presents an overview of the literature relevant to the study. It
²⁴⁴ discusses the biological and computational foundations underlying mitochondrial
²⁴⁵ genome analysis and assembly, as well as existing tools, algorithms, and techniques
²⁴⁶ related to chimera detection and genome quality assessment. The chapter aims to
²⁴⁷ highlight the strengths, limitations, and research gaps in current approaches that
²⁴⁸ motivate the development of the present study.

²⁴⁹ **2.1 The Mitochondrial Genome**

²⁵⁰ Mitochondrial genome (mtDNA) is a small, typically circular molecule found in
²⁵¹ most eukaryotes. It encodes essential genes involved in oxidative phosphorylation
²⁵² and energy metabolism. Because of its conserved structure, mtDNA has become
²⁵³ a valuable genetic marker for studies in population genetics and phylogenetics
²⁵⁴ (Anderson et al., 1981; Boore, 1999). In animal species, the mitochondrial genome

ranges from 15–20 kilobase and contains 13 protein-coding genes, 22 tRNAs, and two rRNAs arranged compactly without introns (Gray, 2012). In comparison to nuclear DNA, the ratio of the number of copies of mtDNA is higher and has simple organization which make it particularly suitable for genome sequencing and assembly studies (Dierckxsens et al., 2017).

2.1.1 Mitochondrial Genome Assembly

Mitochondrial genome assembly refers to the reconstruction of the complete mitochondrial DNA (mtDNA) sequence from raw or fragmented sequencing reads. It is conducted to obtain high-quality, continuous representations of the mitochondrial genome that can be used for a wide range of analyses, including species identification, phylogenetic reconstruction, evolutionary studies, and investigations of mitochondrial diseases. Because mtDNA evolves rapidly, its assembled sequence provides valuable insights into population structure, lineage divergence, and adaptive evolution across taxa (Boore, 1999). Compared to nuclear genome assembly, assembling the mitochondrial genome is often considered more straightforward but still encounters technical challenges such as the formation of chimeric reads. Commonly used tools for mitogenome assembly such as GetOrganelle and MITObim operate under the assumption of organelle genome circularity, and are vulnerable when chimeric reads disrupt this circular structure, resulting in assembly errors (Hahn et al., 2013; Jin et al., 2020).

275 2.2 PCR Amplification and Chimera Formation

276 PCR plays an important role in NGS library preparation, as it amplifies target
277 DNA fragments for downstream analysis. However as previously mentioned, the
278 amplification process can also introduce chimeric reads which compromises the
279 quality of the input reads supplied to sequencing or assembly workflows. Chimeras
280 typically arise when incomplete extension occurs during a PCR cycle. This causes
281 the DNA polymerase to switch from one template to another and generate hy-
282 brid recombinant molecules (Judo et al., 1998). Artificial chimeras are produced
283 through such amplification errors, whereas biological chimeras occur naturally
284 through genomic rearrangements or transcriptional events.

285 In the context of amplicon-based sequencing, the presence of chimeras can in-
286 flate estimates of genetic or microbial diversity and may cause misassemblies dur-
287 ing genome reconstruction. Qin et al. (2023) has reported that chimeric sequences
288 may account for more than 10% of raw reads in amplicon datasets. This artifact
289 tends to be most prominent among rare operational taxonomic units (OTUs) or
290 singletons, which are sometimes misinterpreted as novel diversity, further caus-
291 ing the complication of microbial diversity analyses (Gonzalez, Zimmermann, &
292 Saiz-Jimenez, 2004). As such, determining and minimizing PCR-induced chimera
293 formation is vital for improving the quality of mitochondrial genome assemblies,
294 and ensuring the reliability of amplicon sequencing data.

295 **2.3 Existing Traditional Approaches for Chimera**

296 **Detection**

297 Several computational tools have been developed to identify chimeric sequences in
298 NGS datasets. These tools generally fall into two categories: reference-based and
299 de novo approaches. Reference-based chimera detection, also known as database-
300 dependent detection, is one of the earliest and most widely used computational
301 strategies for identifying chimeric sequences in amplicon-based community studies.
302 These methods rely on the comparison of each query sequence against a curated,
303 high-quality database of known, non-chimeric reference sequences (Edgar et al.,
304 2011).

305 On the other hand, the de novo chimera detection, also referred to as reference-
306 free detection, represents an alternative computational paradigm that identifies
307 chimeric sequences without reliance on external reference databases. This method
308 infer chimeras based on internal relationships among the sequences present within
309 the dataset itself, making it particularly advantageous in studies of under explored
310 or taxonomically diverse communities where comprehensive reference databases
311 are unavailable or incomplete (Edgar, 2016; Edgar et al., 2011). The underlying
312 assumption on this method is that during PCR, true biological sequences are
313 generally more abundant as they are amplified early and dominate the read pool,
314 whereas chimeric sequences appear later and are generally less abundant. The
315 de novo approach leverage this abundance hierarchy, treating the most abundant
316 sequences as supposed parents and testing whether less abundant sequences can
317 be reconstructed as mosaics of these templates. Compositional and structural
318 similarity are also evaluated to check whether different regions of a candidate

319 sequence correspond to distinct high-abundance sequences.

320 In practice, many modern bioinformatics pipelines combine both paradigms
321 sequentially: an initial de novo step identifies dataset-specific chimeras, followed
322 by a reference-based pass that removes remaining artifacts relative to established
323 databases (Edgar, 2016). These two methods of detection form the foundation of
324 tools such as UCHIME and later UCHIME2.

325 2.3.1 UCHIME

326 UCHIME is one of the most widely used tools for detecting chimeric sequences in
327 amplicon-based studies and remains a standard quality-control step in microbial
328 community analysis. Its core strategy is to test whether a query sequence (Q) can
329 be explained as a mosaic of two parent sequences, (A and B), and to score this
330 relationship using a structured alignment model (Edgar et al., 2011).

331 In reference mode, UCHIME divides the query into several segments and maps
332 them against a curated database of non-chimeric sequences. Candidate parents
333 are identified, and a three-way alignment is constructed. The algorithm assigns
334 “Yes” votes when different segments of the query match different parents and
335 “No” votes when the alignment contradicts a chimeric pattern. The final score
336 reflects the balance of these votes. In de novo mode, UCHIME operationalizes the
337 abundance-skew principle described earlier: high-abundance sequences are treated
338 as candidate parents, and lower-abundance sequences are evaluated as potential
339 mosaics. This makes the method especially useful when no reliable reference
340 database exists.

341 Although UCHIME is highly sensitive, it faces key constraints. Chimeras
342 formed from parents with very low divergence (below 0.8%) are difficult to detect
343 because they are nearly indistinguishable from sequencing errors. Accuracy in ref-
344 erence mode depends strongly on database completeness, while de novo detection
345 assumes that true parents are both present and sufficiently more abundant, such
346 conditions are not always met.

347 **2.3.2 UCHIME2**

348 UCHIME2 extends the original algorithm with refinements tailored for high-
349 resolution sequencing data. One of its major contributions is a re-evaluation
350 of benchmarking practices. Edgar (2016) demonstrated that earlier accuracy es-
351 timates for chimera detection were overly optimistic because they relied on un-
352 realistic scenarios where all true parent sequences were assumed to be present.
353 Using the more rigorous CHSIMA benchmark, UCHIME2 showed the prevalence
354 of “fake models” or real biological sequences that can be perfectly reconstructed
355 as apparent chimeras of other sequences, which suggests that perfect chimera de-
356 tection is theoretically unattainable. UCHIME2 also introduces several preset
357 modes (e.g., denoised, balanced, sensitive, specific, high-confidence) designed to
358 tune sensitivity and specificity depending on dataset characteristics. These modes
359 allow users to adjust the algorithm to the expected noise level or analytical goals.

360 Despite these improvements, UCHIME2 must be applied with caution. The
361 author’s website manual (Edgar, n.d) explicitly advises against using UCHIME2
362 as a standalone chimera-filtering step in OTU clustering or denoising workflows
363 because doing so can inflate both false positives and false negatives.

364 2.3.3 CATch

365 As previously mentioned, UCHIME (Edgar et al., 2011) relied on alignment-based
366 sequences in amplicon data. However, researchers soon observed that different al-
367 gorithms often produced inconsistent predictions. A sequence might be identified
368 as chimeric by one tool but classified as non-chimeric by another, resulting in
369 unreliable filtering outcomes across studies.

370 To address these inconsistencies, Mysara, Saeys, Leys, Raes, and Monsieurs
371 (2015) developed the Classifier for Amplicon Tool Chimeras (CATCh), which rep-
372 resents the first ensemble machine learning system designed for chimera detection
373 in 16S rRNA amplicon sequencing. Rather than depending on a single detec-
374 tion strategy, CATCh integrates the outputs of several established tools, includ-
375 ing UCHIME, ChimeraSlayer, DECIPHER, Pintail, and Perseus. The individual
376 scores and binary decisions generated by these tools are used as input features for
377 a supervised learning model. The algorithm employs a Support Vector Machine
378 (SVM) with a Pearson VII Universal Kernel (PUK) to determine optimal weight-
379 ings among the input features and to assign each sequence a probability of being
380 chimeric.

381 Benchmarking in both reference-based and de novo modes demonstrated signif-
382 icant performance improvements. CATCh achieved sensitivities of approximately
383 85 percent in reference-based mode and 92 percent in de novo mode, with corre-
384 sponding specificities of approximately 96 percent and 95 percent. These results
385 indicate that CATCh detected 7 to 12 percent more chimeras than any individual
386 algorithm while maintaining high precision.

387 2.3.4 ChimPipe

388 Among the available tools for chimera detection, ChimPipe is a pipeline developed
389 to identify chimeric sequences such as biological chimeras. It uses both discordant
390 paired-end reads and split-read alignments to improve the accuracy and sensitivity
391 of detecting biological chimeras (Rodriguez-Martin et al., 2017). By combining
392 these two sources of information, ChimPipe achieves better precision than meth-
393 ods that depend on a single type of indicator.

394 The pipeline works with many eukaryotic species that have available genome
395 and annotation data (Rodriguez-Martin et al., 2017). It can also predict multiple
396 isoforms for each gene pair and identify breakpoint coordinates that are useful
397 for reconstructing and verifying chimeric transcripts. Tests using both simulated
398 and real datasets have shown that ChimPipe maintains high accuracy and reliable
399 performance.

400 ChimPipe lets users adjust parameters to fit different sequencing protocols or
401 organism characteristics. Experimental results have confirmed that many chimeric
402 transcripts detected by the tool correspond to functional fusion proteins, demon-
403 strating its utility for understanding chimera biology and its potential applications
404 in disease research (Rodriguez-Martin et al., 2017).

405 2.4 Machine Learning Approaches for Chimera 406 and Sequence Quality Detection

Traditional chimera detection tools rely primarily on heuristic or alignment-based rules. Recent advances in machine learning (ML) have demonstrated that models trained on sequence-derived features can effectively capture compositional and structural patterns in biological sequences. Although most existing ML systems such as those used for antibiotic resistance prediction, taxonomic classification, or viral identification are not specifically designed for chimera detection, they highlight how data-driven models can outperform similarity-based heuristics by learning intrinsic sequence signatures. In principle, ML frameworks can integrate indicators such as k-mer frequencies, GC-content variation and split-alignment metrics to identify subtle anomalies that may indicate a chimeric origin (Arango et al., 2018; Liang, Bible, Liu, Zou, & Wei, 2020; Ren et al., 2020).

2.4.1 Feature-Based Representations of Genomic Sequences

420 Feature extraction converts DNA sequences into numerical representations suit-
421 able for machine learning models. One approach is k-mer frequency analysis,
422 which counts short nucleotide sequences within a read (Vervier, Mahé, Tournoud,
423 Veyrieras, & Vert, 2015). High-frequency k-mers, including simple repeats such
424 as “AAAAAA,” can highlight repetitive or unusual regions that may occur near
425 chimeric junctions. Comparing k-mer patterns across adjacent parts of a read can
426 help identify such regions, while GC content provides an additional descriptor of

427 local sequence composition (Ren et al., 2020).

428 Alignment-derived features further inform junction detection. Long-read tools
429 such as Sniffles (Sedlazeck et al., 2018) use split alignments to locate breakpoints
430 across extended sequences, whereas short-read aligners like Minimap2 (Li, 2018)
431 report supplementary and secondary alignments that indicate local discontinu-
432 ities. Split alignments, where parts of a read map to different regions, can reveal
433 template-switching events. These features complement k-mer profiles and en-
434 hance detection of potentially chimeric reads, even in datasets with incomplete
435 references.

436 Microhomology, or short sequences shared between adjacent segments, is an-
437 other biologically meaningful feature. Its length, typically a few to tens of base
438 pairs, has been linked to microhomology-mediated repair and template-switching
439 mechanisms (Sfeir & Symington, 2015). In PCR-induced chimeras, short iden-
440 tical sequences at junctions provide a clear signature of chimerism. Measuring
441 the longest exact overlap at each breakpoint complements k-mer and alignment
442 features and helps identify reads that are potentially chimeric.

443 2.5 Synthesis of Chimera Detection Approaches

444 To provide an integrated overview of the literature discussed in this chapter, Ta-
445 ble 2.1 summarizes the major chimera detection studies, their methodological
446 approaches, and their known limitations.

Table 2.1: Comparison of Chimera Detection Approaches and Tools

Method / Tool	Core Approach	Key Limitations
Reference-based Detection	Compares each query sequence against curated databases of verified, non-chimeric sequences; evaluates segment similarity to identify mosaic patterns.	Accuracy depends on database completeness; performs poorly for novel taxa or missing parents; limited sensitivity for low-divergence chimeras.
De novo Detection	Identifies chimeras using only internal dataset structure; leverages abundance hierarchy and compositional similarity to infer whether low-abundance sequences can be reconstructed from abundant parents.	Assumes true sequences are more abundant; fails when amplification bias distorts abundances; struggles when parental sequences are similarly abundant or highly similar.
UCHIME	Alignment-based model that partitions the query into segments, identifies parent candidates, and computes a chimera score via a three-way alignment; supports reference and de novo modes.	Reduced accuracy for very closely related parents (<0.8% divergence); sensitive to incomplete databases; de novo mode fails if parents are absent or not sufficiently more abundant.
UCHIME2	Updated UCHIME with improved benchmarking (CHSIMA) and multiple sensitivity/specificity presets; better handles incomplete references and dataset variability.	“Fake models” limit theoretical accuracy; genuine variants may mimic chimeras; not recommended as a standalone step in OTU or denoising pipelines due to increased false positives/negatives.
CATCh	First ensemble ML model for 16S chimera detection; integrates outputs of UCHIME, ChimeraSlayer, DECIPHER, Pintail, and Perseus using an SVM to boost overall prediction accuracy.	Performance constrained by underlying tools; ML model cannot capture features not present in component algorithms; may misclassify in highly novel or low-coverage datasets.
ChimPipe	Pipeline for detecting biological chimeras in RNA-seq using discordant paired-end reads and split-read alignments; identifies isoforms and breakpoint coordinates.	Requires high-quality genome and annotation; tailored to RNA-seq rather than amplicons; computationally intensive; limited to organisms with available reference genomes.

447 Across existing studies, no single approach reliably detects all forms of chimeric
448 sequences, and the reviewed literature consistently shows that chimeras remain a
449 persistent challenge in genomics and bioinformatics. Although the surveyed tools
450 are not designed specifically for organelle genome assembly, they provide valua-
451 ble insights into which methodological strategies are effective and where current
452 approaches fall short. These limitations collectively define a clear research gap:
453 the need for a specialized, feature-driven detection framework tailored to PCR-
454 induced mitochondrial chimeras. Addressing this gap aligns with the research
455 objective outlined in Section 1.3, which is to develop and evaluate a machine
456 learning-based pipeline (MitoChime) that improves the quality of downstream
457 mitochondrial genome assembly. In support of this aim, the subsequent chapters
458 describe the design, implementation, and evaluation of the proposed tool.

⁴⁵⁹ **Chapter 3**

⁴⁶⁰ **Research Methodology**

⁴⁶¹ This chapter outlines the steps involved in completing the study, including data
⁴⁶² gathering, generating simulated mitochondrial Illumina reads, preprocessing and
⁴⁶³ indexing the data, developing a feature extraction pipeline to extract key features,
⁴⁶⁴ applying machine learning algorithms for chimera detection, and validating and
⁴⁶⁵ comparing model performance.

⁴⁶⁶ **3.1 Research Activities**

⁴⁶⁷ As illustrated in Figure 3.1, this study carried out a sequence of procedures to
⁴⁶⁸ detect PCR-induced chimeric reads in mitochondrial genomes. The process began
⁴⁶⁹ with collecting a mitochondrial reference sequence of *Sardinella lemuru* from the
⁴⁷⁰ National Center for Biotechnology Information (NCBI) database, which was used
⁴⁷¹ as a reference for generating simulated clean and chimeric reads. These reads
⁴⁷² were subsequently indexed and mapped. The resulting collections then passed

473 through a feature extraction pipeline that extracted k-mer profiles, supplementary
474 alignment (SA) features, and microhomology information to prepare the data for
475 model construction. The machine learning model was trained using the processed
476 input, and its precision and accuracy were assessed. It underwent tuning until it
477 reached the desired performance threshold, after which it proceeded to validation
478 and will undergo testing.

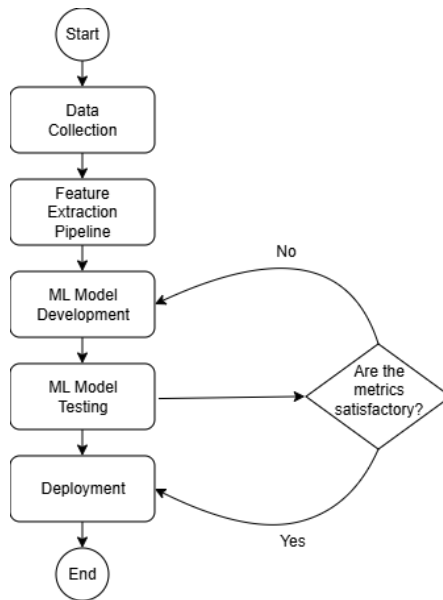


Figure 3.1: Process Diagram of Special Project

479 3.1.1 Data Collection

480 The mitochondrial genome reference sequence of *S. lemuru* was obtained from the
481 NCBI database (accession number NC_039553.1) in FASTA format. This sequence
482 served as the basis for generating simulated reads for model development.

483 This step was scheduled to begin in the first week of November 2025 and
484 expected to be completed by the end of that week, with a total duration of ap-

485 proximately one (1) week.

486 Data Preprocessing

487 To reduce manual repetition, all steps in the simulation and preprocessing pipeline
488 were executed using a custom script in Python (Version 3.11). The script runs
489 each stage, including read simulation, reference indexing, mapping, and alignment
490 processing, in a fixed sequence.

491 Sequencing data were simulated from the NCBI reference genome using `wgsim`
492 (Version 1.13). First, a total of 10,000 paired-end fragments were simulated,
493 producing 20,000 reads (10,000 forward and 10,000 reverse) from the the original
494 reference (`original_reference.fasta`) and and designated as clean reads using
495 the command:

```
496 wgsim -1 150 -2 150 -r 0 -R 0 -X 0 -e 0.001 -N 10000 \  
497     original_reference.fasta ref1.fastq ref2.fastq
```

498 The command parameters are as follows:

- 499 • `-1` and `-2`: read lengths of 150 base pairs for each paired-end read.
- 500 • `-r`, `-R`, `-X`: mutation rate, fraction of indels, and indel extension probability,
501 all set to a default value of 0.
- 502 • `-e`: base error rate, set to 0.001 to simulate realistic sequencing errors.
- 503 • `-N`: number of read pairs, set to 10,000.

504 Chimeric sequences were then generated from the same NCBI reference using a
505 separate Python script. Two non-adjacent segments were randomly selected such
506 that their midpoint distances fell within specified minimum and maximum thresh-
507 olds. The script attempts to retain microhomology, or short identical sequences
508 at segment junctions, to mimic PCR-induced template switching. The resulting
509 chimeras were written to `chimera_reference.fasta`, with headers recording seg-
510 ment positions and microhomology length. The `chimera_reference.fasta` was
511 processed with `wgsim` to simulate 10,000 paired-end fragments, generating 20,000
512 chimeric reads (10,000 forward reads in `chimeric1.fastq` and 10,000 reverse reads
513 in `chimeric2.fastq`) using the command format.

514 Next, a `minimap2` index of the reference genome was created using:

```
515 minimap2 -d ref.mmi original_reference.fasta
```

516 Minimap2 (Version 2.28) is a tool used to map reads to a reference genome.
517 The index `ref.mmi` of the original reference sequence is required by `minimap2` for
518 efficient read mapping. Mapping allows extraction of alignment features from each
519 read, which were used as input for the machine learning model. The simulated
520 clean and chimeric reads were then mapped to the reference index as follows:

```
521 minimap2 -ax sr -t 8 ref.mmi ref1.fastq ref2.fastq > clean.sam
```

```
522 minimap2 -ax sr -t 8 ref.mmi \  
523 chimeric1.fastq chimeric2.fastq > chimeric.sam
```

524 Here, `-ax sr` specifies short-read alignment mode, and `-t 8` uses 8 CPU

525 threads. The resulting clean and chimeric SAM files contain the alignment posi-
526 tions of each read relative to the original reference genome.

527 The SAM files were then converted to BAM format, sorted, and indexed using

528 `samtools` (Version 1.20):

```
529 samtools view -bS clean.sam -o clean.bam  
530 samtools view -bS chimeric.sam -o chimeric.bam  
531  
532 samtools sort clean.bam -o clean.sorted.bam  
533 samtools index clean.sorted.bam  
534  
535 samtools sort chimeric.bam -o chimeric.sorted.bam  
536 samtools index chimeric.sorted.bam
```

537 BAM files are the compressed binary version of SAM files, which enables faster
538 processing and reduced storage. Sorting arranges reads by genomic coordinates,
539 and indexing allows detection of SA as a feature for the machine learning model.

540 The total number of simulated reads was expected to be 40,000. The final col-
541 lection of reads contained 19,984 clean reads and 20,000 chimeric reads (39,984 en-
542 tries in total), providing a roughly balanced distribution between the two classes.
543 After alignment with `minimap2`, only 19,984 clean reads remained because un-
544 mapped reads were not included in the BAM file. Some sequences failed to align
545 due to the 5% error rate defined during `wgsim` simulation, which produced mis-
546 matches that caused certain reads to fall below the aligner's matching threshold.

547 This whole process was scheduled to start in the second week of November 2025

548 and was expected to be completed by the last week of November 2025, with a total
549 duration of approximately three (3) weeks.

550 3.1.2 Feature Extraction Pipeline

551 This stage directly follows the previous alignment phase, utilizing the resulting
552 BAM files (specifically `chimeric.sorted.bam` and `clean.sorted.bam`). A custom
553 Python script was created to efficiently process each primary-mapped read to
554 extract the necessary set of analytical features, which are then compiled into a
555 structured feature matrix in TSV format. The pipeline's core functionality relies on
556 libraries, namely `Pysam` (Version 0.22) for the robust parsing of BAM structures and
557 `NumPy` (Version 1.26) for array operations and computations. To ensure correctness
558 and adherence to best practices, bioinformatics experts at the PGC Visayas will
559 be consulted to validate the pipeline design, feature extraction logic, and overall
560 data integrity. This stage of the study was scheduled to begin in the last week
561 of November 2025 and conclude by the first week of December 2025, with an
562 estimated total duration of approximately two (2) weeks.

563 The pipeline focuses on three features that collectively capture biological sig-
564 natures associated with PCR-induced chimeras: (1) Supplementary alignment flag
565 (SA count), (2) k-mer composition difference, and (3) microhomology.

566 Supplementary Alignment Flag

567 Split-alignment information was derived from the `SA` (Supplementary Alignment)
568 tag embedded in each primary read of the BAM file. This tag is typically asso-

569 ciated with reads that map to multiple genomic locations, suggesting a chimeric
570 structure. To extract this information, the script first checked whether the read
571 carried an SA:Z tag. If present, the tag string was parsed using the function
572 `parse_sa_tag`, yielding a structure for each alignment containing the reference
573 name, mapped position, strand, mapping quality, and number of mismatches.

574 After parsing, the function `sa_feature_stats` was applied to establish the fun-
575 damental split indicators, `has_sa` and `sa_count`. Along with these initial counts,
576 the function synthesized a summarization by aggregating metrics related to the
577 structure and reliability of the split alignments.

578 K-mer Composition Difference

579 Chimeric reads often comprise fragments from distinct genomic regions, resulting
580 in a compositional discontinuity between segments. Comparing k-mer frequency
581 profiles between the left and right halves of a read allows for the detection of such
582 abrupt compositional shifts, independent of alignment information.

583 The script implemented this by inferring a likely junction breakpoint using
584 the function `infer_breakpoints`, prioritizing the boundaries defined by soft-
585 clipping operations in the CIGAR string. If no clipping was present, the midpoint
586 of the alignment or the read length was utilized as a fallback. The read sequence
587 was then divided into left and right segments at this inferred breakpoint, and
588 k-mer frequency profiles ($k = 5$) were generated for both halves, ignoring any
589 k-mers containing ambiguous 'N' bases. The resulting k-mer frequency vectors
590 will be normalized and compared using the functions `cosine_difference` and
591 `js_divergence`.

592 **Microhomology**

593 The process of extracting the microhomology feature started by utilizing the func-
594 tion `infer_breakpoints` similar to the k-mer workflow. Once a breakpoint was es-
595 tablished, the script scanned a ± 40 base pair window surrounding the breakpoint
596 and used the function `longest_suffix_prefix_overlap` to identify the longest
597 exact suffix-prefix overlap between the left and right read segments. This overlap,
598 which represents consecutive bases shared at the junction, was recorded as the
599 `microhomology_length` in the dataset. The 40-base pair window was chosen to
600 ensure that short shared sequences at or near the breakpoint were captured, with-
601 out including distant sequences that are unrelated. Additionally, the GC content
602 of the overlapping sequence was calculated using the function `gc_content`, which
603 counts guanine (G) and cytosine (C) bases within the detected microhomology
604 and divides by the total length, yielding a proportion between 0 and 1, and was
605 stored under the `microhomology_gc` attribute. Short microhomologies, typically
606 3-20 base pairs in length, are recognized signatures of PCR-induced template
607 switching (Peccoud et al., 2018).

608 A k-mer length of 6 was used to capture patterns within the same 40-base pair
609 window surrounding each breakpoint. These profiles complement microhomology
610 measurements and help identify junctions that are potentially chimeric.

611 **3.1.3 Machine Learning Model Development**

612 After feature extraction, the per-read feature matrices for clean and chimeric
613 reads were merged into a single dataset. Each row corresponded to one paired-

614 end read, and columns encoded alignment-structure features (e.g., supplementary
615 alignment count and spacing between segments), CIGAR-derived soft-clipping
616 statistics (e.g., left and right soft-clipped length, total clipped bases), k-mer com-
617 position discontinuity between read segments, and microhomology descriptors
618 near candidate junctions. The resulting feature set was restricted to quantities
619 that can be computed from standard BAM/FASTQ files in typical mitochondrial
620 sequencing workflows.

621 The labelled dataset was randomly partitioned into training (80%) and test
622 (20%) subsets using stratified sampling to preserve the 1:1 ratio of clean to
623 chimeric reads. Model development and evaluation were implemented in Python
624 (Version 3.11) using the `scikit-learn`, `xgboost`, `lightgbm`, and `catboost` li-
625 braries. A broad panel of classification algorithms was then benchmarked on the
626 training data to obtain a fair comparison of different model families under identical
627 feature conditions. The panel included: a trivial dummy classifier, L_2 -regularized
628 logistic regression, a calibrated linear support vector machine (SVM), k -nearest
629 neighbours, Gaussian Naïve Bayes, decision-tree ensembles (Random Forest, Ex-
630 tremely Randomized Trees, and Bagging with decision trees), gradient boosting
631 methods (Gradient Boosting, XGBoost, LightGBM, and CatBoost), and a shallow
632 multilayer perceptron (MLP).

633 For each model, five-fold stratified cross-validation was performed on the train-
634 ing set. In every fold, four-fifths of the data were used for fitting and the remaining
635 one-fifth for validation. Mean cross-validation accuracy, precision, recall, F1-score
636 for the chimeric class, and area under the receiver operating characteristic curve
637 (ROC–AUC) were computed to summarize performance and rank candidate meth-
638 ods. This baseline screen allowed comparison of linear, probabilistic, neural, and

639 ensemble-based approaches and identified tree-based ensemble and boosting mod-
640 els as consistently strong performers relative to simpler baselines.

641 **3.1.4 Model Benchmarking, Hyperparameter Optimiza-
642 tion, and Evaluation**

643 Model selection and refinement proceeded in two stages. First, the cross-validation
644 results from the broad panel were used to identify a subset of competitive mod-
645 els for more detailed optimization. Specifically, ten model families were carried
646 forward: L_2 -regularized logistic regression, calibrated linear SVM, Random For-
647 est, ExtraTrees, Gradient Boosting, XGBoost, LightGBM, CatBoost, Bagging
648 with decision trees, and a shallow MLP. This subset spans both linear and non-
649 linear decision boundaries, but emphasizes ensemble and boosting methods, which
650 showed superior F1 and ROC–AUC in the initial benchmark.

651 Second, hyperparameter optimization was conducted for each of the ten se-
652 lected models using randomized search with five-fold stratified cross-validation
653 (`RandomizedSearchCV`). For tree-based ensembles, the search space included the
654 number of trees, maximum depth, minimum samples per split and leaf, and the
655 fraction of features considered at each split. For boosting methods, key hyper-
656 parameters such as the number of boosting iterations, learning rate, tree depth,
657 subsampling rate, and column subsampling rate were tuned. For the MLP, the
658 number and size of hidden layers, learning rate, and L_2 -regularization strength
659 were varied. In all cases, the primary optimisation criterion was the F1-score of
660 the chimeric class, averaged across folds.

661 For each model family, the hyperparameter configuration with the highest
662 mean cross-validation F1-score was selected as the best-tuned estimator. These
663 tuned models were then refitted on the full training set and evaluated once on the
664 held-out test set to obtain unbiased estimates of performance. Test-set metrics in-
665 cluded accuracy, precision, recall, F1-score for the chimeric class, and ROC–AUC.
666 Confusion matrices and ROC curves were generated for the top-performing mod-
667 els to characterise common error modes, such as false negatives (missed chimeric
668 reads) and false positives (clean reads incorrectly labelled as chimeric). The final
669 model or small set of models for downstream interpretation was chosen based on
670 a combination of test-set F1-score, ROC–AUC, and practical considerations such
671 as model complexity and ease of deployment within a feature extraction pipeline.

672 **3.1.5 Feature Importance and Interpretation**

673 To relate model decisions to biologically meaningful signals, feature-importance
674 analyses were performed on the best-performing tree-based models. Two comple-
675 mentary approaches were used. First, built-in importance measures from ensemble
676 methods (e.g., split-based importances in Random Forest and Gradient Boosting)
677 were examined to obtain an initial ranking of features based on their contribution
678 to reducing impurity. Second, model-agnostic permutation importance was com-
679 puted on the test set by repeatedly permuting each feature column while keeping
680 all others fixed and measuring the resulting decrease in F1-score. Features whose
681 permutation led to a larger performance drop were interpreted as more influential
682 for chimera detection.

683 For interpretability, individual features were grouped into four conceptual

684 families: (i) supplementary alignment and alignment-structure features (e.g., SA
685 count, spacing between alignment segments, strand consistency), (ii) CIGAR-
686 derived soft-clipping features (e.g., left and right soft-clipped length, total clipped
687 bases), (iii) k-mer composition discontinuity features (e.g., cosine distance and
688 Jensen–Shannon divergence between k-mer profiles of read segments), and (iv) mi-
689 crohomology descriptors (e.g., microhomology length and local GC content around
690 putative breakpoints). Aggregating permutation importance scores within each
691 family allowed assessment of which biological signatures contributed most strongly
692 to the classifier’s performance. This analysis provided a basis for interpreting the
693 trained models in terms of known mechanisms of PCR-induced template switching
694 and for identifying which alignment- and sequence-derived cues are most informa-
695 tive for distinguishing chimeric from clean mitochondrial reads.

696 3.1.6 Validation and Testing

697 Validation will involve both internal and external evaluations. Internal valida-
698 tion was achieved through five-fold cross-validation on the training data to verify
699 model generalization and reduce variance due to random sampling. External vali-
700 dation will be achieved through testing on the 20% hold-out dataset derived from
701 the simulated reads, which will be an unbiased benchmark to evaluate how well
702 the trained models generalized to unseen data. All feature extraction and prepro-
703 cessing steps were performed using the same feature extraction pipeline to ensure
704 consistency and comparability across validation stages.

705 Comparative evaluation was performed across all candidate algorithms, in-
706 cluding a trivial dummy classifier, L_2 -regularized logistic regression, a calibrated

707 linear SVM, k-nearest neighbours, Gaussian Naïve Bayes, decision-tree ensembles,
708 gradient boosting methods, and a shallow MLP. This evaluation determined which
709 models demonstrated the highest predictive performance and computational effi-
710 ciency under identical data conditions. Their metrics were compared to identify
711 which algorithms were most suitable for further refinement.

712 3.1.7 Documentation

713 Comprehensive documentation was maintained throughout the study to ensure
714 transparency and reproducibility. All stages of the research, including data gath-
715 ering, preprocessing, feature extraction, model training, and validation, were sys-
716 tematically recorded in a .README file in the GitHub repository. For each ana-
717 lytical step, the corresponding parameters, software versions, and command line
718 scripts were documented to enable exact replication of results.

719 The repository structure followed standard research data management prac-
720 tices, with clear directories for datasets and scripts. Computational environments
721 were standardized using Conda, with an environment file (`environment.arm.yml`)
722 specifying dependencies and package versions to maintain consistency across sys-
723 tems.

724 For manuscript preparation and supplementary materials, Overleaf (L^AT_EX)
725 was used to produce publication-quality formatting and consistent referencing.

726 3.2 Calendar of Activities

727 Table 3.1 presents the project timeline in the form of a Gantt chart, where each
728 bullet point corresponds to approximately one week of planned activity.

Table 3.1: Timetable of Activities

Activities (2025)	Nov	Dec	Jan	Feb	Mar	Apr	May
Data Collection and Simulation	• • •						
Feature Extraction Pipeline	•	•					
Machine Learning Development		•	••	• • •	• • •	••	
Testing and Validation						••	• • •
Documentation	• • •	• • •	• • •	• • •	• • •	• • •	• • •

729 Chapter 4

730 Results and Discussion

731 4.1 Descriptive Analysis of Features

732 This chapter presents the performance of the proposed feature set and machine
733 learning models for detecting PCR-induced chimeric reads in simulated mitochon-
734 drial Illumina data. We first describe the behaviour of the main features, then
735 compare baseline classifiers, assess the effect of hyperparameter tuning, and fi-
736 nally analyse feature importance in terms of individual variables and biologically
737 motivated feature families.

738 The final dataset contained 31,986 reads for training and 7,997 reads for test-
739 ing, with classes balanced (approximately 4,000 clean and 4,000 chimeric reads in
740 the test split).

741 4.1.1 Exploratory Data Analysis

742 An exploratory data analysis (EDA) was conducted on the extracted feature ma-
743 trix to characterize general patterns in the data and gain preliminary insight into
744 which variables might meaningfully contribute to classification. Histograms of
745 key features indicated that alignment-based variables showed clear class separa-
746 tion as chimeric reads have higher frequencies of split alignments and no-
747 ticeably broader long-tailed distribution on soft-clipped regions (`softclip_left`
748 and `softclip_right`). In contrast, sequence-based variables such as microhomol-
749 ogy length and k-mer divergence displayed substantial overlap between classes,
750 suggesting more limited discriminative value. The complete set of histograms is
751 provided in Appendix A.

752 As shown in Figure 4.1, the feature correlation heatmap shows that alignment-
753 derived variables form a strongly correlated cluster, whereas sequence-derived
754 measures show weak correlations with both the alignment-based features and with
755 one another. This heterogeneity indicates that no single feature family captures
756 all relevant signal sources.

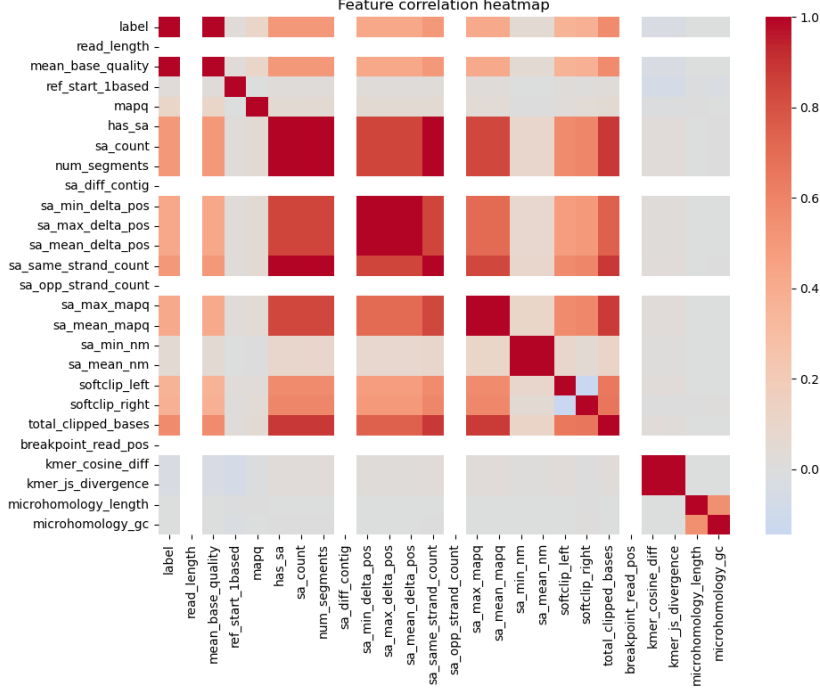


Figure 4.1: Feature correlation heatmap showing relationships among alignment-derived and sequence-derived variables.

757 4.2 Baseline Classification Performance

758 Table 4.1 summarises the performance of eleven classifiers trained on the engi-
 759 neered feature set using five-fold cross-validation and evaluated on the held-out
 760 test set. All models were optimised using default hyperparameters, without ded-
 761 icated tuning.

762 The dummy baseline, which always predicts the same class regardless of the
 763 input features, achieved an accuracy of 0.50 and test F1-score of 0.67. This re-
 764 flects the balanced class distribution and provides a lower bound for meaningful
 765 performance.

766 Across other models, test F1-scores clustered in a narrow band between ap-
 767 proximately 0.74 and 0.77 and ROC–AUC values between 0.82 and 0.84. Gradi-
 768 ent boosting, CatBoost, LightGBM, XGBoost, bagging trees, random forest, and
 769 multilayer perceptron (MLP) all produced very similar scores, with CatBoost and
 770 gradient boosting slightly ahead (test F1 \approx 0.77, ROC–AUC \approx 0.84). Linear
 771 models (logistic regression and calibrated linear SVM) performed only marginally
 772 worse (test F1 \approx 0.74), while Gaussian Naive Bayes lagged behind with substan-
 773 tially lower F1 (\approx 0.65) despite very high precision for the chimeric class.

Table 4.1: Performance of baseline classifiers on the held-out test set.

model	test_accuracy	test_precision	test_recall	test_f1	test_roc_auc
dummy_baseline	0.500000	0.500000	1.000000	0.667000	0.500000
logreg_l2	0.789000	0.945000	0.614000	0.744000	0.821000
linear_svm_calibrated	0.789000	0.945000	0.614000	0.744000	0.820000
random_forest	0.788000	0.894000	0.654000	0.755000	0.834000
extra_trees	0.788000	0.901000	0.647000	0.753000	0.824000
gradient_boosting	0.802000	0.936000	0.648000	0.766000	0.840000
xgboost	0.800000	0.929000	0.650000	0.765000	0.839000
lightgbm	0.799000	0.926000	0.650000	0.764000	0.838000
catboost	0.803000	0.936000	0.650000	0.767000	0.839000
knn	0.782000	0.892000	0.642000	0.747000	0.815000
gaussian_nb	0.741000	0.996000	0.483000	0.651000	0.819000
bagging_trees	0.792000	0.900000	0.657000	0.760000	0.837000
mlp	0.789000	0.931000	0.625000	0.748000	0.819000

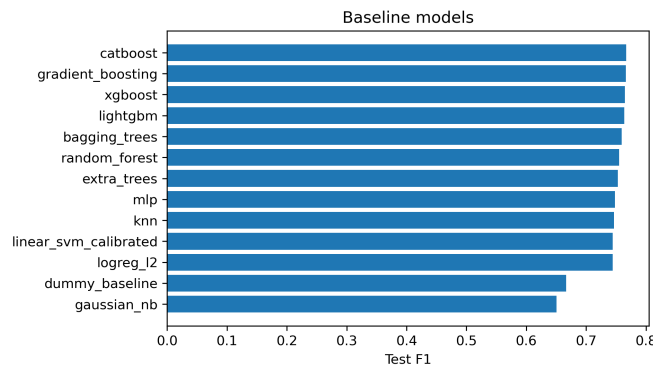


Figure 4.2: Test F1 of all baseline classifiers, showing that no single model clearly dominates and several achieve comparable performance.

774 4.3 Effect of Hyperparameter Tuning

775 To assess whether performance could be improved further, ten model families un-
776 derwent randomised hyperparameter search (Chapter 3). The tuned metrics are
777 summarised in Table 4.2. Overall, tuning yielded modest but consistent gains for
778 tree-based ensembles and boosting methods, while leaving linear models essen-
779 tially unchanged or slightly worse.

780 CatBoost, gradient boosting, LightGBM, XGBoost, random forest, bagging
781 trees, and MLP all experienced small increases in test F1 (typically $\Delta F1 \approx 0.002$ –
782 0.009) and ROC–AUC (up to $\Delta AUC \approx 0.008$). After tuning, CatBoost remained
783 the best performer with test accuracy 0.802, precision 0.924, recall 0.658, F1-score
784 0.769, and ROC–AUC 0.844. Gradient boosting achieved almost identical perfor-
785 mance (F1 0.767, AUC 0.843). Random forest and bagging trees also improved
786 to F1 scores around 0.763 with AUC ≈ 0.842 .

Table 4.2: Performance of tuned classifiers on the held-out test set.

model	test_accuracy	test_precision	test_recall	test_f1	test_roc_auc
logreg_l2_tuned	0.788000	0.946000	0.612000	0.743000	0.818000
linear_svm_calibrated_tuned	0.788000	0.944000	0.612000	0.743000	0.818000
random_forest_tuned	0.797000	0.915000	0.655000	0.763000	0.842000
extra_trees_tuned	0.794000	0.910000	0.652000	0.760000	0.837000
gradient_boosting_tuned	0.802000	0.928000	0.654000	0.767000	0.843000
xgboost_tuned	0.799000	0.922000	0.653000	0.765000	0.839000
lightgbm_tuned	0.801000	0.930000	0.651000	0.766000	0.842000
catboost_tuned	0.802000	0.924000	0.658000	0.769000	0.844000
bagging_trees_tuned	0.798000	0.922000	0.650000	0.763000	0.842000
mlp_tuned	0.790000	0.934000	0.625000	0.749000	0.821000

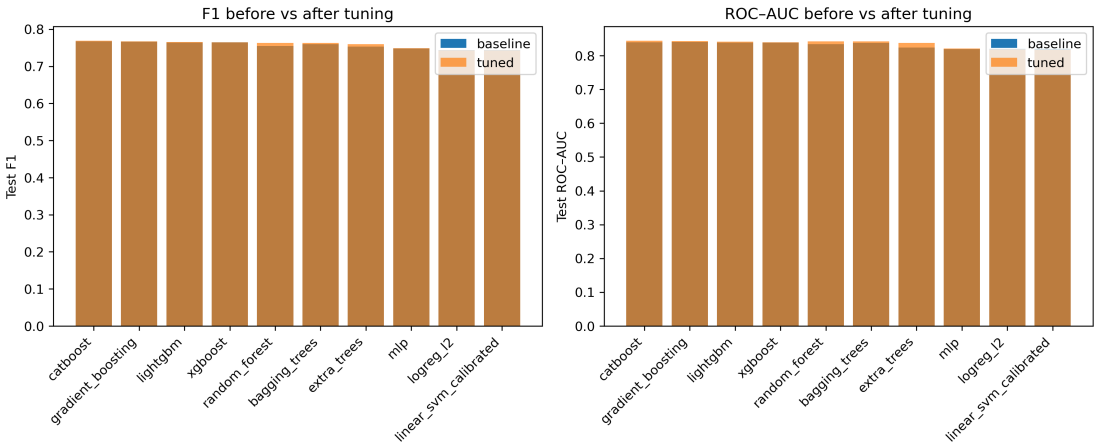


Figure 4.3: Comparison of test F1 (left) and ROC–AUC (right) for baseline and tuned models. Hyperparameter tuning yields small but consistent gains, particularly for tree-based ensembles.

787 Because improvements are small and within cross-validation variability, we
 788 interpret tuning as stabilising and slightly refining the models rather than funda-
 789 mentally altering their behaviour or their relative ranking.

790 4.4 Detailed Evaluation of Representative Mod- 791 els

792 For interpretability and diversity, four tuned models were selected for deeper
 793 analysis: CatBoost (best-performing boosted tree), scikit-learn gradient boost-
 794 ing (canonical gradient-boosting implementation), random forest (non-boosted
 795 ensemble baseline), and L_2 -regularised logistic regression (linear baseline). All
 796 models were trained on the engineered feature set and evaluated on the same
 797 held-out test data.

798 4.4.1 Confusion Matrices and Error Patterns

799 Classification reports and confusion matrices for the four models reveal consistent
800 patterns. CatBoost and gradient boosting both reached overall accuracy of ap-
801 proximately 0.80 with similar macro-averaged F1 scores (~ 0.80). For CatBoost,
802 precision and recall for clean reads were 0.73 and 0.95, respectively, while for
803 chimeric reads they were 0.92 and 0.66 ($F1 = 0.77$). Gradient boosting showed
804 nearly identical trade-offs.

805 Random forest attained slightly lower accuracy (0.80) and chimeric F1 (0.76),
806 whereas logistic regression achieved the lowest accuracy among the four (0.79)
807 and chimeric F1 (0.74), although it provided the highest chimeric precision (0.95)
808 at the cost of lower recall (0.61).

809 Across all models, errors were asymmetric. False negatives (chimeric reads
810 predicted as clean) were more frequent than false positives. For example, CatBoost
811 misclassified 1 369 chimeric reads as clean but only 215 clean reads as chimeric.
812 This pattern indicates that the models are conservative: they prioritise avoiding
813 spurious chimera calls at the expense of missing some true chimeras. Depending on
814 downstream application, alternative decision thresholds or cost-sensitive training
815 could be explored to adjust this balance.

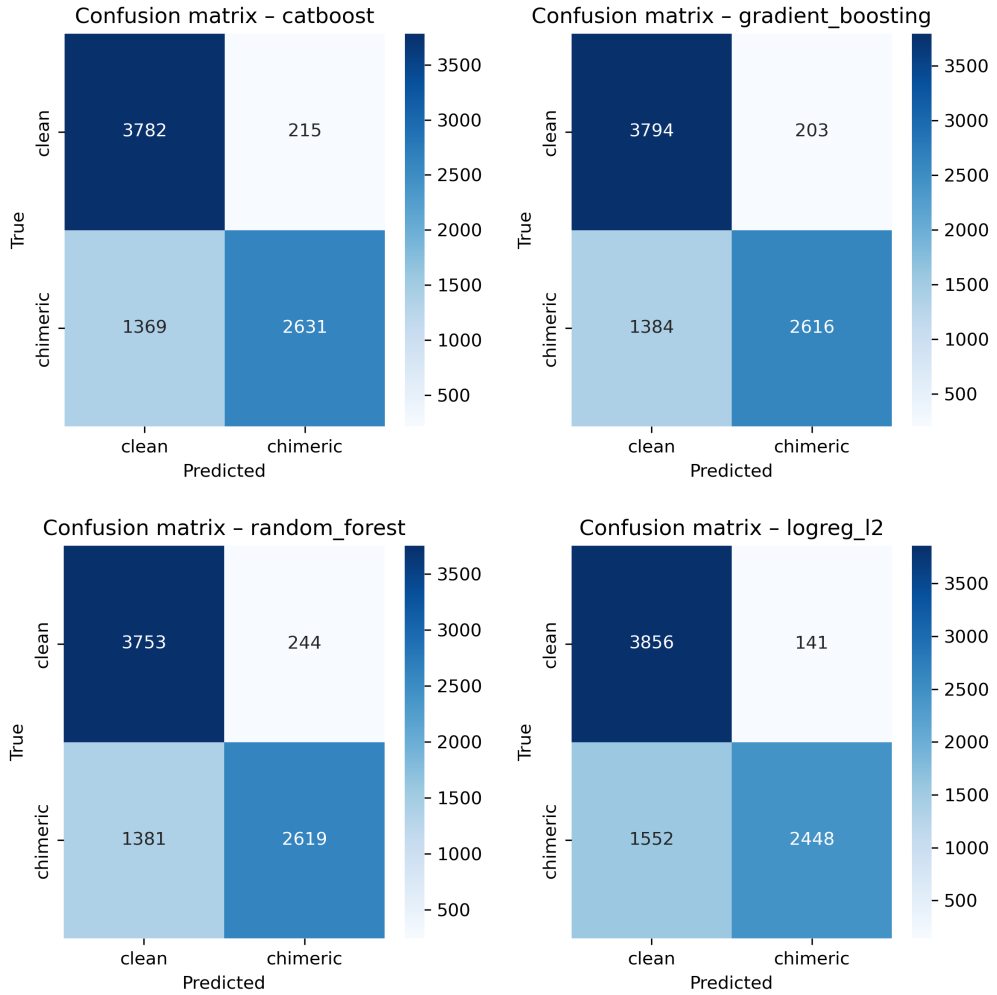


Figure 4.4: Confusion matrices for the four representative models on the held-out test set. All models show more false negatives (chimeric reads called clean) than false positives.

816 4.4.2 ROC and Precision–Recall Curves

817 Receiver operating characteristic (ROC) and precision–recall (PR) curves (Fig-
 818 ure 4.5) further support the similarity among the top models. The three tree-based
 819 ensembles (CatBoost, gradient boosting, random forest) achieved ROC–AUC val-
 820 ues of approximately 0.84 and average precision (AP) around 0.88. Logistic re-

821 gression performed slightly worse ($AUC \approx 0.82$, $AP \approx 0.87$) but still substantially
822 better than random guessing.

823 The PR curves show that precision remains above 0.9 across a broad range
824 of recall values (up to roughly 0.5–0.6), after which precision gradually declines.
825 This behaviour indicates that the models can assign very high confidence to a
826 subset of chimeric reads, while more ambiguous reads can only be recovered by
827 accepting lower precision.

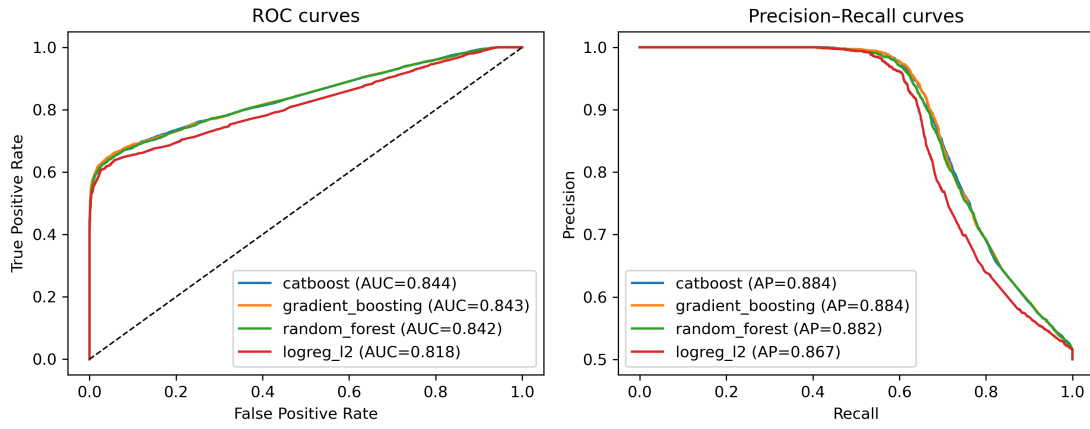


Figure 4.5: ROC (left) and precision–recall (right) curves for the four representative models on the held-out test set. Tree-based ensembles cluster closely, with logistic regression performing slightly but consistently worse.

828 **4.5 Feature Importance and Biological Interpre-**
829 **tation**

830 **4.5.1 Permutation Importance of Individual Features**

831 To understand how each classifier made predictions, feature importance was quan-
832 tified using permutation importance. In this approach, the values of a single fea-
833 ture are randomly shuffled, and the resulting drop in F_1 score (ΔF_1) reflects how
834 strongly the model depends on that feature. Greater decreases in F_1 indicate
835 stronger reliance on that feature. This analysis was applied to four representa-
836 tive models: CatBoost, Gradient Boosting, Random Forest, and L_2 -regularized
837 Logistic Regression.

838 As shown in Figure 4.6, the total number of clipped bases consistently pro-
839 vides a strong predictive signal, particularly in Random Forest, Gradient Boosting,
840 and L_2 -regularized Logistic Regression. CatBoost differs by assigning the highest
841 importance to k-mer divergence metrics such as `kmer_js_divergence`, which cap-
842 ture subtle sequence changes resulting from structural variants or PCR-induced
843 chimeras. Soft-clipping features (`softclip_left` and `softclip_right`) provide
844 additional context around breakpoints, complementing these primary signals in
845 all models except Gradient Boosting. L_2 -regularized Logistic Regression relies
846 more on alignment-based split-read metrics when breakpoints are simple, but it is
847 less effective at detecting complex rearrangements that introduce novel sequences.

848 Overall, these results indicate that accurate detection of chimeric reads relies
849 on both alignment-based signals and k-mer compositional information. Explicit

850 microhomology features contribute minimally in this analysis, and combining both
 851 alignment-based and sequence-level features enhances model sensitivity and speci-
 852 ficiency.

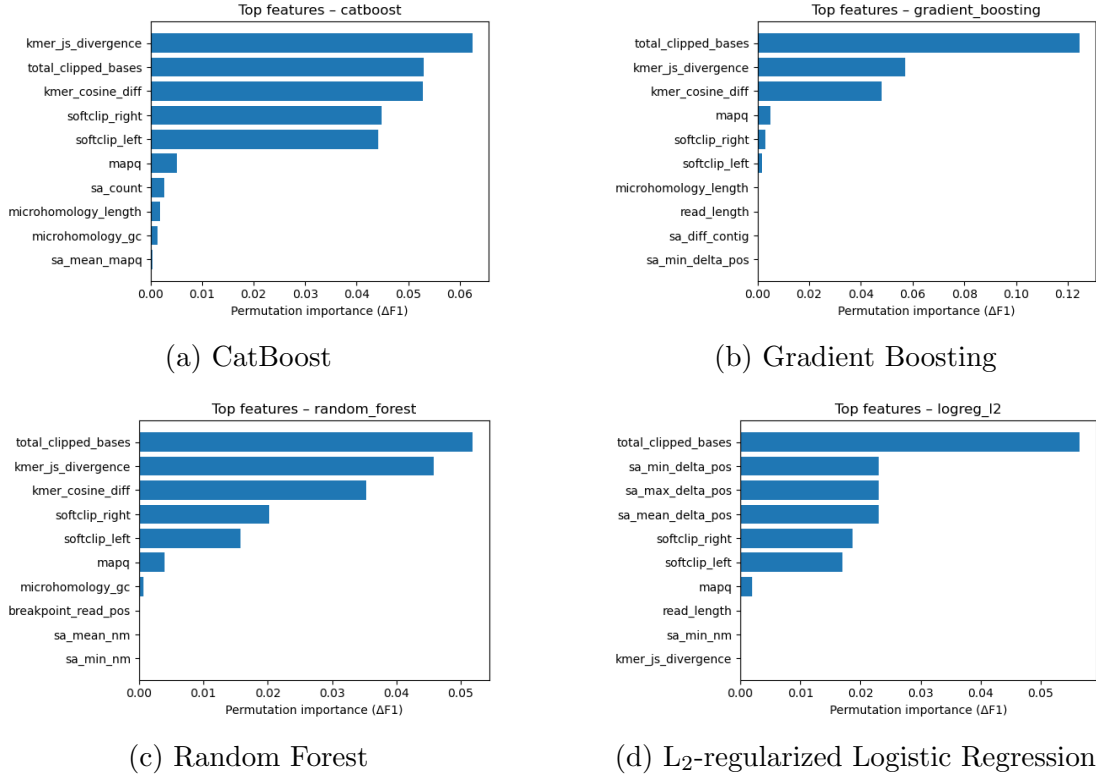


Figure 4.6: Permutation-based feature importance for four representative classifiers. Clipping and k-mer composition features are generally the strongest predictors, whereas microhomology and other alignment metrics contribute minimally.

853 4.5.2 Feature Family Importance

854 To evaluate the contribution of broader biological signals, features were
 855 grouped into five families: SA_structure (supplementary alignment and seg-
 856 ment metrics, e.g., has_sa, sa_count, sa_min_delta_pos, sa_mean_nm), Clipping
 857 (softclip_left, softclip_right, total_clipped_bases, breakpoint_read_pos),

858 Kmer_jump (`kmer_cosine_diff`, `kmer_js_divergence`), Micro_homology, and
859 Other (e.g., `mapq`).

860 Aggregated analyses reveal consistent patterns across models. In CatBoost,
861 the Clipping family has the largest cumulative contribution (0.14), followed
862 by Kmer_jump (0.12), with Other features contributing modestly (0.005) and
863 SA_structure (0.003) and Micro_homology (0.003) providing minimal predictive
864 power. Gradient Boosting shows a similar trend, with Clipping (0.13) domi-
865 nating, Kmer_jump (0.11) secondary, and the remaining families contributing
866 negligibly. Random Forest integrates both Clipping (0.088) and Kmer_jump
867 (0.08) effectively, while SA_structure, Micro_homology, and Other remain minor
868 contributors. L₂-regularized Logistic Regression emphasizes Clipping (0.09)
869 and SA_structure (0.07), with Kmer_jump and Micro_homology having minimal
870 impact.

871 Both feature-level and aggregated analyses indicate that detection of chimeric
872 reads in this dataset relies primarily on alignment disruptions (Clipping) and
873 k-mer compositional shifts (Kmer_jump), which often arise from PCR-induced
874 recombination events, while explicit microhomology features contribute minimally.

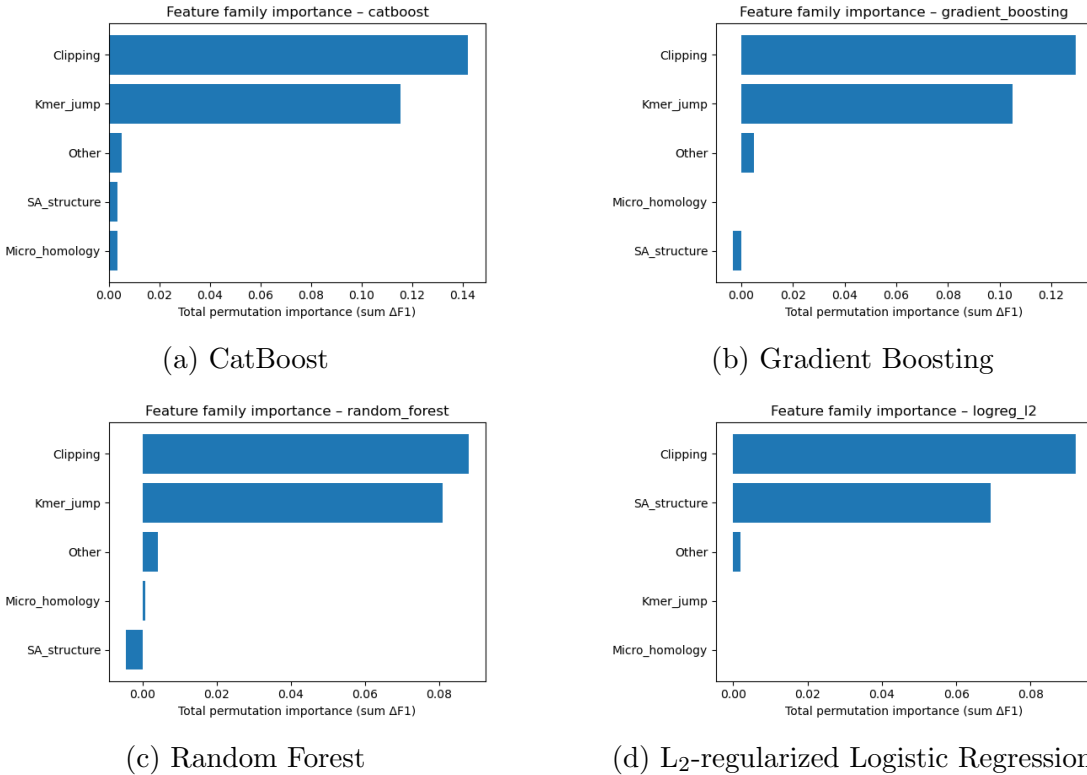


Figure 4.7: Aggregated feature family importance across four models. Clipping and k-mer compositional shifts are consistently the dominant contributors, while SA_structure, Micro_homology, and other features contribute minimally.

875 4.6 Summary of Findings

876 After removing trivially discriminative metadata, all models performed substan-
 877 tially better than the dummy baseline, with test F1-scores around 0.76 and ROC-
 878 AUC values near 0.84. Hyperparameter tuning yielded modest improvements,
 879 with boosting methods, particularly CatBoost and gradient boosting, achieving
 880 the highest performance. Confusion matrices and precision-recall curves indicate
 881 that these models prioritise precision for chimeric reads while accepting lower re-
 882 call, which a conservative strategy appropriate for scenarios where false positives

883 are costly.

884 Feature importance analyses revealed that alignment disruptions, such as clip-
885 ping, and abrupt k-mer composition changes accounted for most predictive power.
886 In contrast, microhomology metrics and supplementary alignment descriptors con-
887 tributed minimally. These results indicate that features based on read alignment
888 and k-mer composition are sufficient to train classifiers for detecting mitochon-
889 drial PCR-induced chimera reads, without needing additional quality-score or
890 positional information in the conditions tested.

891 **Appendix A**

892 **Exploratory Data Analysis**

893 **A.1 Histograms of Key Features**

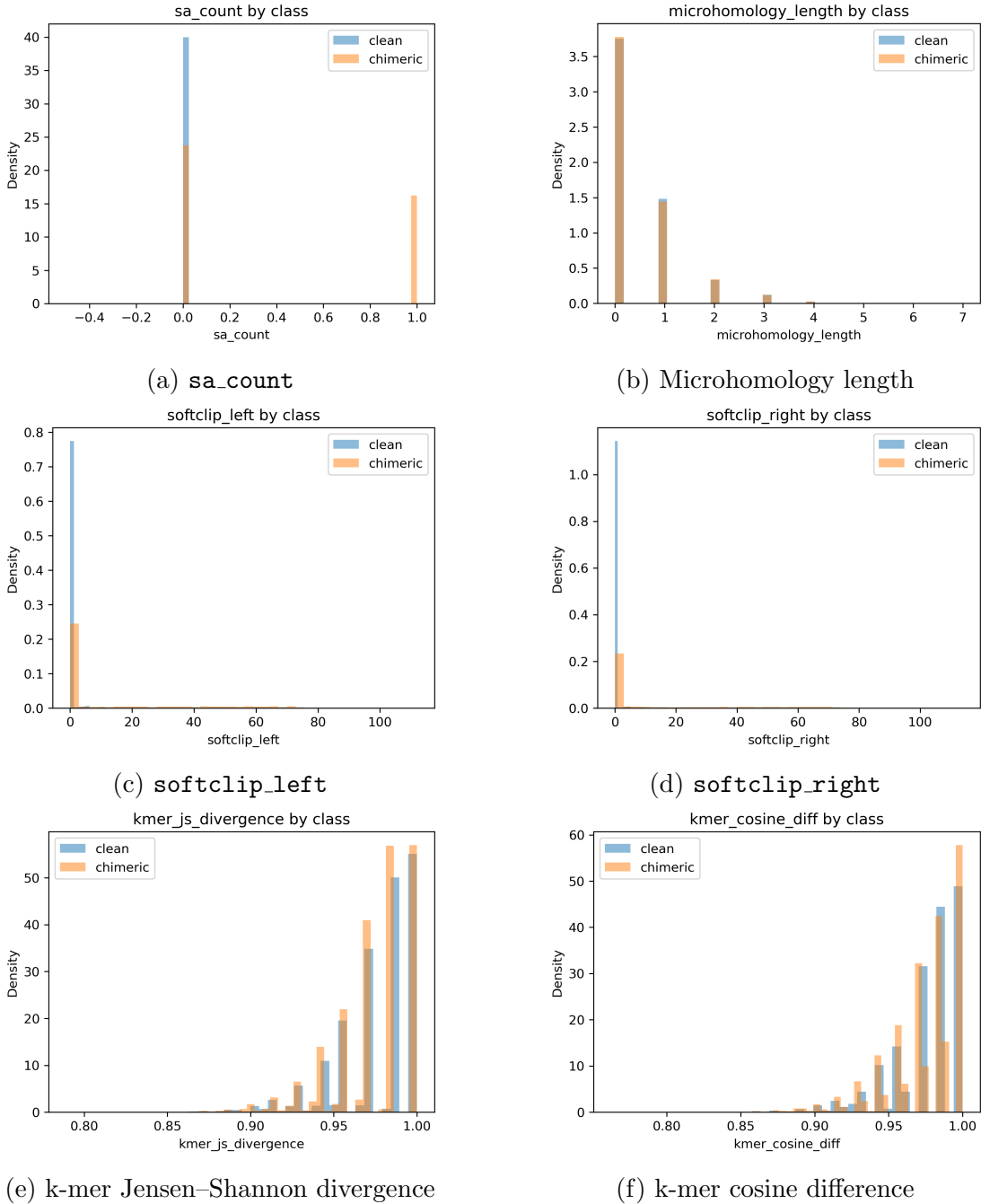


Figure A.1: Histogram plots of six key features comparing clean and chimeric reads.

894 References

- 895 Anderson, S., Bankier, A., Barrell, B., Bruijn, M., Coulson, A., Drouin, J., ...
896 Young, I. (1981, 04). Sequence and organization of the human mitochondrial
897 genome. *Nature*, *290*, 457-465. doi: 10.1038/290457a0
898 Arango, G., Garner, E., Pruden, A., Heath, L., Vikesland, P., & Zhang, L. (2018,
899 02). Deeparg: A deep learning approach for predicting antibiotic resistance
900 genes from metagenomic data. *Microbiome*, *6*. doi: 10.1186/s40168-018
901 -0401-z
902 Bentley, D. R., Balasubramanian, S., Swerdlow, H. P., Smith, G. P., Milton, J.,
903 Brown, C. G., ... Smith, A. J. (2008). Accurate whole human genome
904 sequencing using reversible terminator chemistry. *Nature*, *456*(7218), 53–
905 59. doi: 10.1038/nature07517
906 Boore, J. L. (1999). Animal mitochondrial genomes. *Nucleic Acids Research*,
907 *27*(8), 1767–1780. doi: 10.1093/nar/27.8.1767
908 Cameron, S. L. (2014). Insect mitochondrial genomics: Implications for evolution
909 and phylogeny. *Annual Review of Entomology*, *59*, 95–117. doi: 10.1146/
910 annurev-ento-011613-162007
911 Dierckxsens, N., Mardulyn, P., & Smits, G. (2017). Novoplasty: de novo assembly
912 of organelle genomes from whole genome data. *Nucleic Acids Research*,

- 913 45(4), e18. doi: 10.1093/nar/gkw955
- 914 Edgar, R. C. (2016). Uchime2: improved chimera prediction for amplicon se-
915 quencing. *bioRxiv*. Retrieved from <https://api.semanticscholar.org/>
- 916 CorpusID:88955007
- 917 Edgar, R. C. (n.d.). *Uchime in practice*. Retrieved from https://www.drive5.com/usearch/manual7/uchime_practical.html
- 918
- 919 Edgar, R. C., Haas, B. J., Clemente, J. C., Quince, C., & Knight, R. (2011).
920 Uchime improves sensitivity and speed of chimera detection. *Bioinformatics*,
921 27(16), 2194–2200. doi: 10.1093/bioinformatics/btr381
- 922 Glenn, T. C. (2011). Field guide to next-generation dna sequencers. *Molecular
923 Ecology Resources*, 11(5), 759–769. doi: 10.1111/j.1755-0998.2011.03024.x
- 924 Gonzalez, J. M., Zimmermann, J., & Saiz-Jimenez, C. (2004, 09). Evalu-
925 ating putative chimeric sequences from pcr-amplified products. *Bioin-
926 formatics*, 21(3), 333-337. Retrieved from <https://doi.org/10.1093/bioinformatics/bti008>
927 doi: 10.1093/bioinformatics/bti008
- 928 Gray, M. W. (2012). Mitochondrial evolution. *Cold Spring Harbor perspectives
929 in biology*, 4. Retrieved from <https://doi.org/10.1101/cshperspect.a011403>
930 doi: 10.1101/cshperspect.a011403
- 931 Hahn, C., Bachmann, L., & Chevreux, B. (2013). Reconstructing mitochondrial
932 genomes directly from genomic next-generation sequencing reads—a baiting
933 and iterative mapping approach. *Nucleic Acids Research*, 41(13), e129. doi:
934 10.1093/nar/gkt371
- 935 Jin, J.-J., Yu, W.-B., Yang, J., Song, Y., dePamphilis, C. W., Yi, T.-S., & Li,
936 D.-Z. (2020). Getorganelle: a fast and versatile toolkit for accurate de
937 novo assembly of organelle genomes. *Genome Biology*, 21(1), 241. doi:
938 10.1186/s13059-020-02154-5

- 939 Judo, M. S. B., Wedel, W. R., & Wilson, B. H. (1998). Stimulation and sup-
940 pression of pcr-mediated recombination. *Nucleic Acids Research*, *26*(7),
941 1819–1825. doi: 10.1093/nar/26.7.1819
- 942 Labrador, K., Agmata, A., Palermo, J. D., Ravago-Gotanco, R., & Pante, M. J.
943 (2021). Mitochondrial dna reveals genetically structured haplogroups of
944 bali sardinella (sardinella lemuru) in philippine waters. *Regional Studies in*
945 *Marine Science*, *41*, 101588. doi: 10.1016/j.rsma.2020.101588
- 946 Li, H. (2018, 05). Minimap2: pairwise alignment for nucleotide sequences. *Bioin-*
947 *formatics*, *34*(18), 3094-3100. Retrieved from <https://doi.org/10.1093/bioinformatics/bty191>
948 doi: 10.1093/bioinformatics/bty191
- 949 Liang, Q., Bible, P. W., Liu, Y., Zou, B., & Wei, L. (2020, 02). Deepmi-
950 crobes: taxonomic classification for metagenomics with deep learning. *NAR*
951 *Genomics and Bioinformatics*, *2*(1), lqaa009. Retrieved from <https://doi.org/10.1093/nargab/lqaa009> doi: 10.1093/nargab/lqaa009
- 952 Metzker, M. L. (2010). Sequencing technologies — the next generation. *Nature*
953 *Reviews Genetics*, *11*(1), 31–46. doi: 10.1038/nrg2626
- 954 Mysara, M., Saeys, Y., Leys, N., Raes, J., & Monsieurs, P. (2015). Catch,
955 an ensemble classifier for chimera detection in 16s rrna sequencing stud-
956 ies. *Applied and Environmental Microbiology*, *81*(5), 1573-1584. Retrieved
957 from <https://journals.asm.org/doi/abs/10.1128/aem.02896-14> doi:
958 10.1128/AEM.02896-14
- 959 Peccoud, J., Lequime, S., Moltini-Conclois, I., Giraud, I., Lambrechts, L., &
960 Gilbert, C. (2018, 04). A survey of virus recombination uncovers canon-
961 ical features of artificial chimeras generated during deep sequencing li-
962 brary preparation. *G3 Genes—Genomes—Genetics*, *8*(4), 1129-1138. Re-
963 trieved from <https://doi.org/10.1534/g3.117.300468> doi: 10.1534/

- 965 g3.117.300468
- 966 Qin, Y., Wu, L., Zhang, Q., Wen, C., Nostrand, J. D. V., Ning, D., ... Zhou, J.
967 (2023). Effects of error, chimera, bias, and gc content on the accuracy of
968 amplicon sequencing. *mSystems*, 8(6), e01025-23. Retrieved from <https://journals.asm.org/doi/abs/10.1128/msystems.01025-23> doi: 10.1128/
969 msystems.01025-23
- 970
- 971 Qiu, X., Wu, L., Huang, H., McDonel, P. E., Palumbo, A. V., Tiedje, J. M., &
972 Zhou, J. (2001). Evaluation of pcr-generated chimeras, mutations, and het-
973 eroduplexes with 16s rrna gene-based cloning. *Applied and Environmental*
974 *Microbiology*, 67(2), 880–887. doi: 10.1128/AEM.67.2.880-887.2001
- 975 Ren, J., Song, K., Deng, C., Ahlgren, N., Fuhrman, J., Li, Y., ... Sun, F. (2020,
976 01). Identifying viruses from metagenomic data using deep learning. *Quan-*
977 *titative Biology*, 8. doi: 10.1007/s40484-019-0187-4
- 978 Rodriguez-Martin, B., Palumbo, E., Marco-Sola, S., Griebel, T., Ribeca, P.,
979 Alonso, G., ... Djebali, S. (2017, 01). Chimpipe: Accurate detection of
980 fusion genes and transcription-induced chimeras from rna-seq data. *BMC*
981 *Genomics*, 18. doi: 10.1186/s12864-016-3404-9
- 982 Rognes, T., Flouri, T., Nichols, B., Quince, C., & Mahé, F. (2016). Vsearch: a
983 versatile open source tool for metagenomics. *PeerJ*, 4, e2584. doi: 10.7717/
984 peerj.2584
- 985 Sedlazeck, F., Rescheneder, P., Smolka, M., Fang, H., Nattestad, M., von Haeseler,
986 A., & Schatz, M. (2018, 06). Accurate detection of complex structural
987 variations using single-molecule sequencing. *Nature Methods*, 15. doi: 10
988 .1038/s41592-018-0001-7
- 989 Sfeir, A., & Symington, L. S. (2015). Microhomology-mediated end joining: A
990 back-up survival mechanism or dedicated pathway? *Trends in Biochemical*

- 991 *Sciences*, 40(11), 701-714. Retrieved from <https://www.sciencedirect.com/science/article/pii/S0968000415001589> doi: <https://doi.org/10.1016/j.tibs.2015.08.006>
- 992 Vervier, K., Mahé, P., Tournoud, M., Veyrieras, J.-B., & Vert, J.-P. (2015,
- 993 11). Large-scale machine learning for metagenomics sequence classifica-
- 994 tion. *Bioinformatics*, 32(7), 1023-1032. Retrieved from <https://doi.org/10.1093/bioinformatics/btv683> doi: 10.1093/bioinformatics/btv683
- 995 Willette, D., Bognot, E., Mutia, M. T., & Santos, M. (2011). *Biology and ecology*
- 996 of sardines in the philippines: A review (Vol. 13; Tech. Rep. No. 1). NFRDI
- 997 Technical Paper Series. Retrieved from <https://nfrdi.da.gov.ph/tpjf/etc/Willette%20et%20al.%20Sardines%20Review.pdf>
- 998
- 999
- 1000
- 1001